Automatic Elimination of High Amplitude Artifacts in EEG Signals

Ana Rita Teixeira
University of Aveiro / IEETA IPC/ ESEC
3810 Aveiro, Portugal
Email: ateixeira@ua.pt

Ana Maria Tomé
University of Aveiro / IEETA
3810 Aveiro, Portugal
Email: ana@ieeta.pt

Isabel Maria Santos
University of Aveiro / CINTESIS
3810 Aveiro, Portugal
Email: isabel.santos@ua.pt

***Abstract*—High amplitude artifacts represent a problem during EEG recordings in neuroscience research. Taking this into account, this paper proposes a method to identify high amplitude artifacts with no requirement for visual inspection, electrooculogram (EOG) reference channel or user assigned parameters. A potential solution to the high amplitude artifacts (HAA) elimination is presented based on the blind source separation technique. The assumption underlying the selection of components is that HAA are independent of the EEG signal and different HAA can be generated during the EEG recordings. Therefore, the number of components related to HAA is variable and depends on the processed signal, which means that the method is adaptable to the input signal. The results demonstrate that the proposed method preferably removes the signal associated to the delta band and maintains the EEG signal information in other bands with a high relative precision, thus improving the quality of the EEG signal. A case study with EEG signals obtained during performance on the Halstead Category Test (HCT) is presented. After HAA removal, data analysis revealed an error-related frontal ERP wave: the feedback-related negativity (FRN) in response to feedback stimuli.**

Keywords–BSS; EEG; ERP; Source Selection

I. INTRODUCTION

The electroencephalogram (EEG) signals measured by placing electrodes over the scalp represent the bioelectrical brain activity which may be used, amongst different applications, in neuroscience studies. During the recordings, the EEG signal is, unfortunately, often contaminated with different physiological factors independent of the cerebral activity, which are typically not of interest - assigned artifacts. The artifacts elimination is an important issue in EEG signal processing and is in many studies a prerequisite for the subsequent signal analysis. In many applications, such as brain computer interface (BCI), the features of the EEG signals are used as a command to control devices and the presence of such artifacts can degrade the performance of the system.

There are several EEG waveforms that differ from background EEG rhythms and may be of interest for particular research and clinical assessment aims. A relevant type of waveform that is studied independently from background EEG activity is the event-related potential (ERP). ERPs are deterministic signals, i.e., they are elicited by specific stimuli or events, and not spontaneous like the rhythms, being a transient form of brain activity generated in the brain structures.

Recent studies show that ERP waves can be used for non-muscular BCI control. There are advantages and drawbacks of using ERPs in BCI. The two main advantages are that 1) ERPs are naturally occuring brain responses, which the user produces without any particular training; 2) ERPs occur at short latencies, which is a beneficial property for the throughput of a BCI. However, these advantages are counterbalanced by some drawbacks. Firstly there are large inter-individual differences in ERP latencies and waveforms, requiring the system to be trained to recognize the ERP of a given individual. Another drawback is that ERP waves have so small amplitudes and are dominated by background activity, that makes them difficult to detect to the human eye. Several methods exist to extract the ERP signal from the EEG background. Simple signal processing techniques including averaging over consecutive trials can reveal their shape and allow their analysis if the EEG signal is not corrupted by artifacts, mainly high amplitude artifacts.

The high amplitude artifacts that derive from eye blinking, eye movements and patient movements affect the scalp EEG channels differently. The frontal scalp channels are impacted the most by these kinds of artifacts. Furthermore, these artifacts have a more significant impact on the temporal correlation with frontal scalp signals than the remaining channels. The high amplitude artifact correction can be regarded as a preprocessing method to clean the EEG signal. There are three main ways of dealing with high amplitude artifacts.

1) Prevention:
   Minimize the occurrence of ocular artifacts and patient movements by giving proper instructions to participants. However the ocular artifacts are spontaneous and involuntary, so this is often unavoidable.
2) Epoch Rejection - Manual Method:
   This is a very simple method to eliminate the artifacts in EEG signals. If an artifact exists in an epoch, then the corrupted epoch is removed. Important data will be lost during the removal process, particularly when limited amount of data is available or when a lot of artifacts exist in EEG signals.
3) Elimination of artifacts:
   Different denoising techniques can be used to eliminate artifacts from the EEG signal. This is the best approach for cleaning the EEG because the number of epochs is preserved.

Techniques of Blind Source Separation (BSS) like Independent Components Analysis (ICA) are promising approaches to decompose the EEG signal in independent components able to identify the artifacts. Although there are several proposals in the literature for an automatic selection of components, all of which require free input parameters, a visual inspection by the user or the EOG reference signal is needed.

The methods used to reject sources with high amplitude can be highlighted: with sparsity greater than some threshold [1], [2], the extreme values in amplitude, the probability measure

 ISBN: 978-1-61208-487-9

using the kurtosis value [3], the mutual information and the spectral pattern [1]. In [1], a subsystem to identify artefactual sources is used based in computing ten statistical measures. These measures are computed for each source and some of them involve the EOG signal reference. In [4], a method to find the ICs representing the muscle artifacts is described. The ICs are classified in a descending order according to their respective auto-correlation values and afterwards some decisions to reject sources are made. As the auto-correlation of muscle artifacts is relatively low with respect to that of the EEG signal, the ICs representing the muscle artifacts are expected to be among the last components. In [5] each IC derived by SOBI is then band-pass filtered between $1 - 10$ Hz to create filtered ICs. The Pearson correlation is calculated between the ICs filtered and the accelerometer signal and a threshold is used to eliminate the components with high correlation value. Different EEGLAB plug-ins were also developed to automatic select the artifact components, such as ADJUST [6], FASTER [7] and AAR [3] based in source probability and in kurtosis values.

The component selection based in the correlation based index (CBI) described in [8] and based in radial frontocentral topographic scalp distribution [9] is used in this study. Such approach is able to identify high amplitude artifacts in a fully automatic way without requiring visual inspection, the EOG reference channel or free parameters as input. This study presents a potential solution to the high amplitude artifacts (HAA) elimination. The assumption underlying the selection method is that HAA are independent of the EEG signal and different HAA can be generated during the EEG recordings. Therefore, the number of components related to HAA is variable and dependent on the processed signal, which means that the method is adaptive to the signal. The proposed method reduces the influence of high amplitude artifacts and improves the quality of the EEG allowing to find different ERP waves.

A study case with the Halstead Category Test (HCT) [10] is presented in this paper. Based on the literature, the aim is to find larger negative amplitudes measured maximally at midline fronto-central electrodes - the feedback-related negativity (FRN) wave [11]. The FRN occurs when the feedback does not conform to the user's expectations after the feedback stimuli. It has been established for years that the brain produces specific evoked responses in case of errors. Along that line, a couple of recent studies have proposed to use error-related brain signals in BCI applications [12]. The use of Error Potentials in BCI arises from the observation that this additional information provided automatically by the user could be used to improve the BCI performance, [13]. The results demonstrate the existence of EEG activity recorded in central scalp locations that is related to error processing, namely the FRN. Specifically, the preprocessing data analysis described revealed an FRN wave during performance on the HCT, a well-established neuropsychological measure of non-verbal reasoning, abstract concept formation and cognitive flexibility, which are aspects of the cognitive executive function. Therefore, this preprocessing method shows potential to be used in improving the quality of the EEG signal used in neuroscience studies. In particular, the results can be useful in BCI applications to clean high amplitude artifacts as well as in detection of FRN waves.

This paper is organized as follows. In section II, the blind source separation technique is described and in section III, the new source selection methodology is presented. The experimental procedure is described in section IV and some metrics for algorithm validations are discussed in section V. Finally, results and conclusions are presented in section VI and VII, respectively.

II. Blind Source Separation

The effectiveness of the BSS technique depends on some assumptions, according to the studied problem, such as: independence, linearity, uncorrelatedness, non-gaussianity, among others described in the literature. The more closely the hypotheses advanced by a certain algorithm are satisfied, the better the method is meant to separate the components. Success hence critically depends on good source separation and on correct identification of sources as brain activity or artifact components. In the literature, BSS is considered to be the best approach for artifacts of high signal to noise ratio (SNR), i.e., high amplitude artifacts [14]. Linear Blind Source Separation models can be expressed algebraically as

$$\mathbf{X} = \mathbf{AS} \tag{1}$$

where the sensored EEG data is organized into a $C \times N$ matrix $\mathbf{X}$, representing C the number of channels and N the number of time points; $\mathbf{A}$ is the $C \times C$ mixing matrix and $\mathbf{S}$ is a $C \times N$ matrix of unknown sources or independent components. The goal of BSS or ICA algorithms is to determine the sources and the separation matrix $\mathbf{B}$ given the measured/ sensored signals $\mathbf{X}$. So, the separation equation reads

$$\mathbf{S} = \mathbf{BX} \tag{2}$$

where $\mathbf{B}$ can be defined as the pseudo-inverse of the mixing matrix, i.e., $\mathbf{B} = \mathbf{A}^{\dagger}$.
Most of BSS/ICA algorithms follow a two step procedure to estimate the separation (or de-mixing) matrix [4]. The first step is based on Principal Component Analysis or Singular Value Decomposition (SVD) of the data matrix $\mathbf{X}$ [15]. For the second step different approaches have been proposed [15]. The separation matrix $\mathbf{B}$ is estimated as the product of matrices computed in both steps. For convenience, these steps are reviewed for the Second Order Blind Identification (SOBI) [16].

- With the SVD of the original data $\mathbf{X}$, two $C \times C$ matrices are computed: the eigenvector matrix $\mathbf{V}$ and the diagonal singular value matrix $\mathbf{D}$. Note that a dimension reduction can be performed by reducing the number of singular values and eigenvectors in the corresponding matrices.
- After whitening the original data, i.e., $\mathbf{Z} = \mathbf{D}^{-1}\mathbf{V}^T\mathbf{X}$, L time-delayed correlation matrices are estimated. The approximate join diagonalization of these set of matrices gives an orthogonal matrix $\mathbf{U}$.

The separation matrix is defined as $\mathbf{B} = \mathbf{U}^T\mathbf{D}^{-1}\mathbf{V}^T$ and its pseudo-inverse as $\mathbf{A} = \mathbf{VDU}$. The mandatory parameter of this algorithm is L, the number of matrices of second step. Eventually, the user can decide to perform dimension reduction after the first step by discarding the smallest singular values and corresponding eigenvectors. In this work, the dimension was maintained equal to the number of sensors (channels), i. e. C, and the L is assigned to 100 and the default value of the energy of the components, i.e., the rows of the matrix

 ISBN: 978-1-61208-487-9

S, is equal to one. Therefore, the coefficients of the mixing matrix can be used to decide the relevance of the sources in the respective linearly mixed signal.

III. Source Selection

Source selection, in BSS applications, is the most widely problem reported in the literature [4]. Existing methods for artifact rejection can be separated into hand-optimized, semi-automatic and fully automatic approaches. Semi-automatic approaches require user interaction for ambiguous or outlier components, while fully automated methods were proposed for the classification of artifacts. Whatever is the case, different metrics have been applied directly to the mixing matrix $\mathbf{A}$ or to the sources $\mathbf{S}$ in order to select artifact related components. In this study, as the sources have energy one, the columns of the mixing matrix determines the power distribution of the reconstructed sources over scalp. Given, the mixing matrix $\mathbf{A}$

$$\mathbf{A} = \begin{pmatrix} a_{11} & a_{12} & \dots & a_{1C} \\ a_{21} & a_{22} & \dots & a_{2C} \\ \dots & \dots & & \dots \\ a_{C1} & a_{C2} & \dots & a_{CC} \end{pmatrix} \quad (3)$$

where $a_{ij},\ (1 \leq i, j \leq C)$ is the transfer coefficient from $j-th$ source to the $i-th$ observed channel signal. Each column vector of the matrix $\mathbf{A}$ reflects the power propagating across all scalp channels of the corresponding row of $\mathbf{S}$ (one source). In this work it is proposed a two-step fully automatic source selection procedure. The first step measures the influence, over all scalp, of each source by estimating the following coefficient

$$CBI(j) = \sum_{i=1}^{C} \frac{|a_{ij}|}{\sqrt{a_{i1}^2 + a_{i2}^2 + \dots + a_{iC}^2}} \quad (4)$$

Experimentally it was verified that the plot of CBI values, ordered by decreasing order of magnitude, shows an abrupt decrease on the first five values and then stabilizes. So, the five largest CBI values are initially identified as candidate columns of the matrix $\mathbf{A}$ associated to the high amplitude artifacts. For the sake of simplicity, from now on assume that the columns of $\mathbf{A}$ and the rows of $\mathbf{S}$ are ordered according to the values of the coefficient CBI. Re-writing the mixing model as a sum of outer products

$$\tilde{\mathbf{X}} = \mathbf{AS} = \mathbf{A}_{*1}\mathbf{S}_{1*} + \mathbf{A}_{*2}\mathbf{S}_{2*} + \ldots + \mathbf{A}_{*C}\mathbf{S}_{C*} \quad (5)$$

where the first term on the right side of the equation 5 corresponds to the source spreading, over the scalp,with largest energy; the second term corresponds to the source spreading with the second largest energy and so on. As referred before, the graphical representation the columns of $\mathbf{A}$ is often used by experts to identify visually the artifacts. The second step of the selection procedure is an application of one of the rules used in this context. To find out if a certain source is an artifact related component it is foreseen that it contributes mostly in the frontal region. To confirm if the five selected candidate columns with highest CBI are related to the high amplitude artifact, the power distribution for all selected j columns should verify the condition $|a_{ij} > |a_{kj}|$, $\forall i \in L_1$ and $k \in L_2$ where $L_1 = [Fp1; Fpz; FP2]$ and $L_2 = [F7; F3; Fz; F4; F8]$ Note after the selection of the artefact related sources the original signal is decomposed into the artefact related signal and the clean signal. The reconstructed signal is then obtained without high amplitude artifacts. By the explanation above it is clear that the EEG signal can be expressed as:

$$\mathbf{X} = (\mathbf{A_1} + \mathbf{A_2})\mathbf{S} \quad (6)$$

where $\mathbf{A_1}\ (C \times C)$ is the matrix with columns associated to the EEG activity (Clean Data) and $\mathbf{A_2}\ (C \times C)$ is the matrix with $j \leq 5$ non null columns associated to the high amplitude artifacts activity (HAA Data).

IV. Experimental procedure

A. Participants and Task

Fifty eight EEG signals belonging to 58 participants with 208 trials each were collected with a Neuroscan SynAmps2 amplifier through an Easy-Cap with 26 channels and recorded with the software Scan 4.3 (Neuroscan Systems). EEG was continuously recorded with Ag-AgCl sintered electrodes which were located according to the $10-20$ system. A computerized version of the Halstead Category Test (HCT) was used to assess cognitive executive frontal lobe function. This test is used to measure a person's ability to formulate abstract principles based on receiving feedback after each specific test item. Visual feedback is provided after each trial, to indicate if the participant responded wrong or right.

B. Dataset

For signal analysis, each EEG trial was epoched from $6000\ ms$ prior to response onset to $3000\ ms$ after, leading to a dataset with 208 trials for each of the 58 participants. Note that after $1500\ ms$ of response onset the feedback was provided and the dataset for each participant can be divided considering the conditions wrong and right.

In this study, the Raw Data signal is the filtered EEG between $[1 - 40]$ Hz in frequency, trial by trial, for each participant; the Clean Data signal is the processed Raw Data by SOBI algorithm with full automatic criteria to select the sources associated with the high amplitude artifacts; and the HAA Data is the reconstructed signal with the automatically rejected sources.

C. Algorithm Performance

As mentioned above, the SOBI algorithm is employed to decompose all epochs into two datasets: Clean and HAA Data. The selection of components is fully automatic, adaptable to each epoch allowing the identification of HAA signal. The number of selected components is variable between 0 and 5. Although almost all epochs in the present dataset were corrupted with high amplitude artifacts, there were occasionally epochs without artifact. In epochs without artifacts, no components are selected. In these datasets $\approx 97\%$ of the trials were corrupted with artifacts and the number of selected components in all trials ranged in average between 1.85 ± 0.98. To demonstrate the algorithm performance two distinct cases are discussed: Case 1 - An epoch without artifacts and Case 2 - An epoch with artifacts.

- **Case 1: Epoch without artifact** Figure 1 (a) represents an example of an epoch without artifact (only 1 second is represented). In this case, the algorithm did not select any component. Considering the maximum

peak of the channel $Fp1$, an average head topography centered in the $100\ ms$ window around the peak was constructed, Figure 1 (b), to illustrate that there are no high-amplitude components in this epoch.

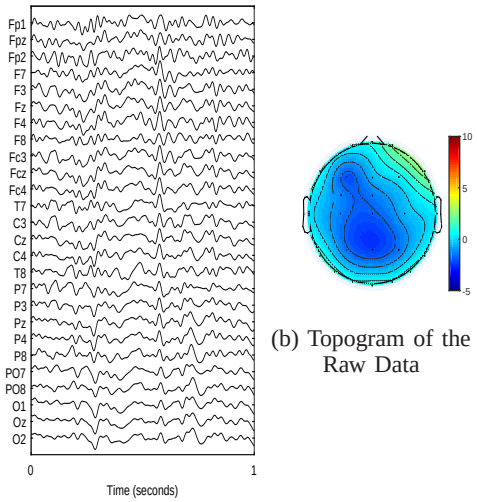

(a) Raw Data

(b) Topogram of the Raw Data

Figure 1. Case 1: (a) Original Epoch - Raw Data (b) Head topography of the corresponding Raw Data considering an average window of $100\ ms$ centered in maximum peak of the $Fp1$ channel.

- **Case 2: Epoch with artifact** In Figure 2 (a) is represented an example of an epoch with an artifact (only 1 second is represented) . In this case, the algorithm selected 4 components (S_{*1}, S_{*3}, S_{*4} and S_{*5}) of the 5 with the largest spread on the scalp. As shown in the head topographies, Figure 2 (d), all components selected by the algorithm have a strong power energy in frontal channels. It should be noted that, although the first component has the highest energy in the frontal channels, the selection is not sufficient to remove the HAA signal, as described in [8] .

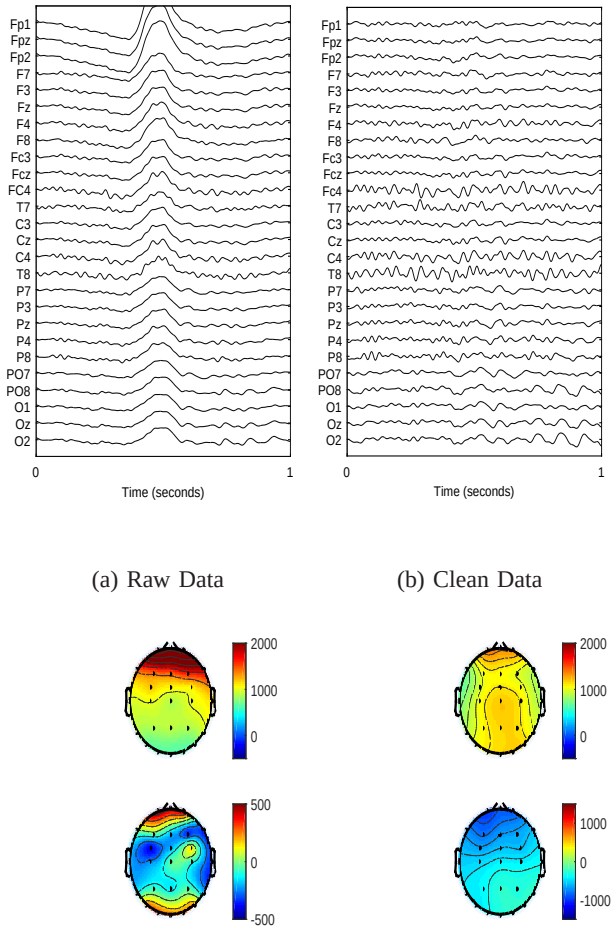

(a) Raw Data

(b) Clean Data

(c) Topograms of the selected IC's.

Figure 2. Case2: (a) Original Epoch - Raw Data (b) Clean Data after HAA signal removed by the automatic proposed method to select the ICs (c) Independent Components obtained by SOBI algorithm (d) Head topography of the selected ICs associated to HAA signal.

V. METRICS FOR ALGORITHM VALIDATION

The efficiency of the automatic method of selection of components was validated using different metrics to compare the Raw Data, the Clean Data and the HAA Data in time and frequency domains in each epoch for all participants. Firstly, the datasets (Raw, Clean and HAA signals) were grouped according to the region of the scalp where the electrodes are located. To account for spatial differences in amplitude distribution, channels were grouped into 6 regions, $R1$: prefrontal channels $(Fp1, Fp2, Fpz)$, $R2$: frontal channels $(F7, F3, Fz, F4, F8)$, $R3$: frontocentral channels $(FC3, FCz, FC4, C3, Cz, C4)$, $R4$: parietal channels $(P7, P3, Pz, P4, P8)$, $R5$: parieto-occipital channels $(PO7, PO8, O1, Oz, O2)$ and $R6$: temporal channels $(T7, T8)$.

The three datasets in each region $(R1-R6)$ were band-pass filtered ($6th$ order Butterworth) , with a zero-phase strategy, into delta: $[1\ \ 4]$ Hz; theta: $[4\ \ 7]$ Hz; alpha: $[7\ \ 13]$ Hz and beta: $[13\ \ 30]$ frequency bands. For all epochs and for all participants, the following metrics were then calculated per band in each region and were performed in three ways: (1) correlation coefficient in time for all signals between: Clean/Raw data; Clean/HAA Data; Raw/HAA Data; (2) coherence of average signal between Clean/Raw Data and Raw/HAA Data and (3) Mean Power to compute relative power between the Clean and Raw Data.

The correlation coefficient was calculated between the Clean/Raw Data, the Clean/HAA Data and the Raw/HAA Data for all bands in all regions, but only region $R5$ is represented in Figure 3. The results show that the Clean/Raw Data has an high correlation in beta, alpha and theta bands and, in turn, Raw/HAA Data presents high correlation in the delta band. Thus, the proposed method reduces the influence of signals

associated to the delta band. Figure 4 presents the results

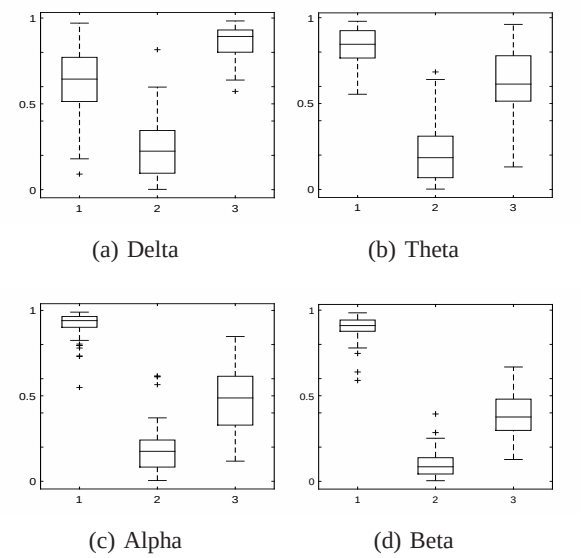

Figure 3. Correlation Coefficient between (1) - Clean/Raw Data ; (2) - Clean/HAA Data ; (3) - Raw/HAA Data in each band for region $R5$

of the computation of the coherence magnitude between the Raw/Clean Data and Raw/HAA Data in regions $R3$ and $R5$. Region $R5$ is less corrupted with artifacts than region $R3$ and because of this the main difference between the results is in delta band values, where the coherence is less than 0.5 in region $R3$ and over 0.5 in region $R5$. In the theta, alpha and beta bands the coherence value for the two datasets is similar in the two regions. These results confirm that the selected components are correlated to the delta bandwidth by ensuring that the remaining frequency bands are unaffected, especially alpha and beta bands. To measure the relation in each band

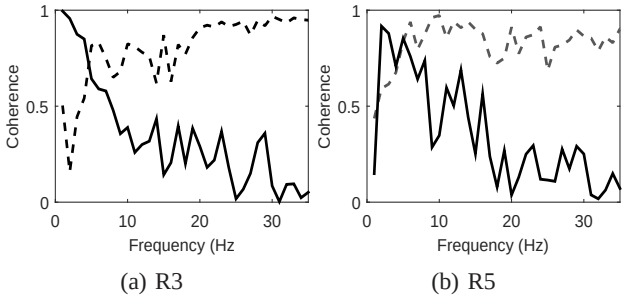

Figure 4. Coherence Magnitude in $R3$ (a) and $R5$ (b) region between the Raw/Clean Data (dash line) and between Raw/HAA Data (solid line).

between the Clean and Raw Data, the relative energy power (RP) for each region was computed as:

$$RP = \frac{\sum_{i=1}^{58} \sum_{n=1}^{9000} x_{c_i}(n)^2}{\sum_{i=1}^{58} \sum_{n=1}^{9000} x_{ri}(n)^2} \quad (7)$$

where x_{c_i} is the Clean Data and x_{r_i} is the Raw Data in each band computed for each region and for all participants $i = 1 : 58$. The results are consistent with the results described above considering the different metrics. The relative power between Clean/Raw Data in region $R3$ is presented in Figure 5. Once again, it can be seen that the band with greater loss of information is the delta band with some 40% and that the alpha and beta bands exhibit residual losses, $\approx 10\%$.

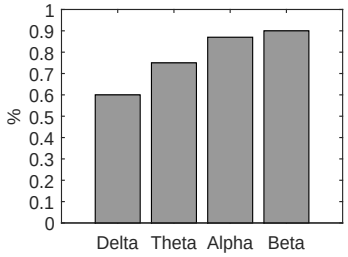

Figure 5. Relative Power between Clean/Raw Data in region $R3$.

VI. Event-Related Potentials

The aim of the current study was to show a new automatic selection algorithm for ICA decompositions to remove high amplitude artifacts in EEG signals. The data used in this study was highly corrupted with artifacts and hence compromises the interpretation of many psychophysiological correlates. In this particular case, the detection of ERP waves associated to performance in the HCT was nearly impossible. To show the impact of the application of this method and its ability to clean the high amplitude artifacts in the signal, the grand average signal of all participants in an average window between $[200 \;\; 300]\; ms$ after the feedback is used, this is depicted in Figure 6 (a). The grand average of the HAA and Clean Data in the same window is also considered, Figures 6 (b) and (c), respectively. The head topographies of the raw data show an high amplitude signal in the frontal channels that mask any ERP wave present. After applying the SOBI algorithm and the automatic component selection, the Clean Data presents a negativity in the central area, that is not evident in the Raw data.

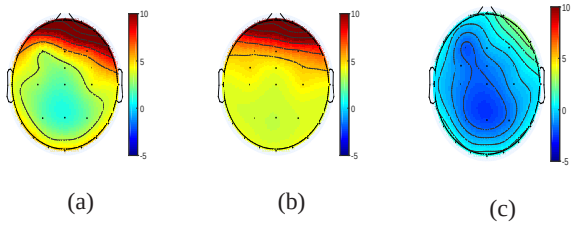

Figure 6. Head topography of the grand average waveforms for all participants considering an average window between $[200 \;\; 300]\; ms$ after the feedback. (a) Raw Data ; (b) HAA Data and (c) Clean Data

A. Feedback-related negativity wave

According to the neuroscience literature, the feedback-related negativity (FRN) is an ERP component recorded in fronto-central areas of the scalp, which originates in the Anterior Cingulate Cortex (ACC) [17]. In this work, all regions were processed but only region $R3$ was chosen to be discussed, because the FRN effects were the strongest on it, in agreement with the existing literature. Figure 7 displays the grand-average

 ISBN: 978-1-61208-487-9

waveforms of individual ERPs for the $R3$ region considering the two subsets of trials corresponding to the Right (ERPr) and Wrong (ERPw) answers, time-locked to the feedback. Thus, the value $0\ ms$ corresponds to the moment when the feedback occurred. In the displayed waveforms, we can observe large negative peaks after the feedback, peaking around $250\ ms$, which are consistent with the feedback-related negativity. As can be observed, the FRN wave in the wrong subset (dash line) is more prominent than in the right subset (solid line). Furthermore, an apparent difference between the Wrong and Right conditions is observed, with more negative amplitudes for the Wrong trials, Figure 7 (b),(c).

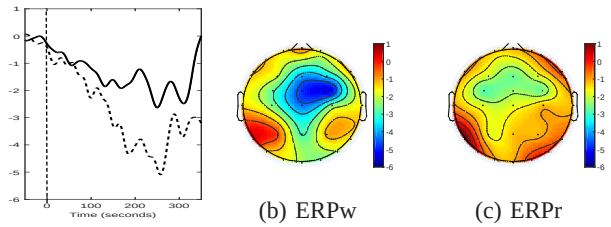

(a) FRN (b) ERPw (c) ERPr

Figure 7. FRN analysis: (a) Grand-average waveforms of individual ERPs in region $R3$ considering two subsets (ERPr and ERPw): Wrong response (dash line) and Right response (solid line). Head topography of the grand-average waveforms considering an average window between $[240\ \ 260]\ ms$ after the feedback: (b) Wrong subset and (c) Right subset

VII. Conclusion

The aim of the component selection method described in this paper is to remove high amplitude artifacts resulting from eye movements, patient movements, etc. It should be noted that this selection method is an alternative to those described in the literature as it is fully automatic and requires no input parameters to work. It is important to highlight the need to reduce the influence of high amplitude artifacts in EEG signals, not only to allow detection of ERP waves in neuroscience studies, but also for use of the EEG in BCI applications. Without doing so, one cannot be sure that the peaks observed in the signal reflect real brain processing and are not confounded with artifacts. After the preprocessing step, the data analysis revealed a frontocentral ERP wave related to error-processing: the feedback-related negativity (FRN), peaking around $250\ ms$, after feedback during performance on the HCT. As expected, errors elicited more negative amplitudes on that potential than correct responses.

Furthermore, results suggest that this error potential, FRN, might provide an adequate method for detecting errors that requires no additional processing time and could thereby improve the speed and accuracy of EEG-based communication with devices using BCI applications. The use of Error Potentials in BCI applications arises from the observation that this additional information provided automatically by the user could be used to improve the BCI performance.

Acknowledgment

This work was supported by FCT grant (Ref:SFRH/BPD/101112/2014)to Ana Rita Teixeira and Bial Foundation grant (Ref: 136/08) to Isabel Santos.

References

[1] M. Kirkove, C. François, and J. Verly, “Comparative evaluation of existing and new methods for correcting ocular artifacts in electroencephalographic recordings,” Signal Processing, vol. 98, may 2014, pp. 102–120.

[2] A. K. Abdullah, C. Z. Zhang, A. A. A. Abdullah, and S. Lian, “Automatic Extraction System for Common Artifacts in EEG Signals Based on Evolutionary Stone’s BSS Algorithm,” Mathematical Problems in Engineering, vol. 2014, aug 2014, pp. 1–25.

[3] A. Delorme, T. Sejnowski, and S. Makeig, “Enhanced detection of artifacts in EEG data using higher-order statistics and independent component analysis.” NeuroImage, vol. 34, no. 4, feb 2007, pp. 1443–9.

[4] L. Albera, A. Kachenoura, P. Comon, A. Karfoul, F. Wendling, L. Senhadji, and I. Merlet, “ICA-Based EEG denoising: a comparative analysis of fifteen methods,” Bulletin of the Polish Academy of Sciences: Technical Sciences, vol. 60, no. 3, jan 2012, pp. 407–418.

[5] I. Daly, M. Billinger, R. Scherer, and G. Muller-Putz, “On the automated removal of artifacts related to head movement from the EEG.” IEEE transactions on neural systems and rehabilitation engineering : a publication of the IEEE Engineering in Medicine and Biology Society, vol. 21, no. 3, may 2013, pp. 427–34.

[6] A. Mognon, J. Jovicich, L. Bruzzone, and M. Buiatti, “ADJUST: An automatic EEG artifact detector based on the joint use of spatial and temporal features.” Psychophysiology, vol. 48, no. 2, feb 2011, pp. 229–40.

[7] H. Nolan, R. Whelan, and R. B. Reilly, “FASTER: Fully Automated Statistical Thresholding for EEG artifact Rejection.” Journal of neuroscience methods, vol. 192, no. 1, sep 2010, pp. 152–62.

[8] W. Kong, Z. Zhou, S. Hu, J. Zhang, F. Babiloni, and G. Dai, “Automatic and direct identification of blink components from scalp EEG.” Sensors (Basel, Switzerland), vol. 13, no. 8, jan 2013, pp. 10 783–801.

[9] M. Silvetti, E. Nuñez Castellar, C. Roger, and T. Verguts, “Reward expectation and prediction error in human medial frontal cortex: an EEG study.” NeuroImage, vol. 84, jan 2014, pp. 376–82.

[10] N. A. DeFilippis and E. McCampbell, The Booklet Category Test. Psychological Assessment Resources, 1997.

[11] M. Falkenstein, J. Hoormann, S. Christ, and J. Hohnsbein, “ERP components on reaction errors and their functional significance: A tutorial,” Biological Psychology, vol. 51, no. 2-3, 2000, pp. 87–107.

[12] P. W. Ferrez and J. del R Millan, “Error-related EEG potentials generated during simulated brain-computer interaction.” IEEE transactions on bio-medical engineering, vol. 55, no. 3, mar 2008, pp. 923–9.

[13] I. Iturrate, L. Montesano, and J. Minguez, “Task-dependent signal variations in EEG error-related potentials for braincomputer interfaces,” Journal of Neural Engineering, vol. 10, no. 2, apr 2013, p. 026024.

[14] I. Daly, N. Nicolaou, S. J. Nasuto, and K. Warwick, “Automated artifact removal from the electroencephalogram: a comparative study.” Clinical EEG and neuroscience, vol. 44, no. 4, oct 2013, pp. 291–306.

[15] A. Tome and E. Lang, “Approximate diagonalization approach to blind source separation with a subset of matrices,” in Seventh International Symposium on Signal Processing and Its Applications, 2003. Proceedings., vol. 2. IEEE, 2003, pp. 105–108 vol.2.

[16] A. Cichocki and S.-i. Amari, Adaptive Blind Signal and Image Processing: Learning Algorithms and Applications, Volume 1, 2002.

[17] W. H. R. Miltner, C. H. Braun, and M. G. H. Coles, “Event-related brain potentials following incorrect feedback in a time-estimation task: Evidence for a generic neural system for error detection,” J. Cognitive Neuroscience, vol. 9, no. 6, 1997, pp. 788–798.

 ISBN: 978-1-61208-487-9